Acquisition of Maneuvring Characteristics of Ships using RANS CFD

Marin Lauber, Pandeli Temarel
Fluid Structure Interctions, University of Southampton, Southampton
M.Lauber@soton.ac.uk

1 Introduction

Numerical predictions of ship manoeuvring have been performed for some time (Oldfield et al. (2016), He et al. (2016), Zou et al. (2010), Kim et al. (2015)). However, the approach undertaken can drastically vary among authors. In addition, commercial computational fluid dynamics (CFD) software allow for a wide range of turbulence models, mesh topologies, free-surface treatments, etc. This yields non-trivial choices and can lead to noticeable differences in the results. In this paper, we investigate the numerical aspects of ship manoeuvring by replicating captive model tests for a benchmark model (KVLCC2) while performing a large range of numerical investigations.

The objectives of this study are:

i) to determine the manoeuvring coefficients of the model by replicating captive model tests (static and dynamic),

ii) to conduct a proper verification of the results, both for temporal and spatial discretization errors,

iii) to conduct a proper validation of the results using experimental data,

iv) to investigate the influence of the turbulence model, mesh and other numerical aspects on the resulting coefficients.

2 Approach

A 1:110 scaled bare model of the KVLCC2 was used in this study. The maneuvring coefficients were obtained by simulating static drift and planar motion mechanism in pure sway and yaw using a Reynolds-Averaged Navier-Stoke (RANS) finite-volume software (Star-CCM$^+$).

Static drift simulations were undertaken at a Froude number (Fr) of 0.142 and drift angles (β) range of $\pm 16°$, in steps of 4°. The domain used extends $5.5L_{PP}$, $2.5L_{PP}$ and $1.2L_{PP}$ in the longitudinal, transverse and vertical direction, respectively. An unstructured hexahedral mesh with local refinements in way of the free-surface, kelvin wake, viscous wake and hull boundary layer was used as standard, see figure 1. To reduce mesh size, wall functions were used to model the boundary layer, with a target non-dimensional wall distance (y^+) of 30. This resulted in a cells count of 3.4M for the standard mesh. The boundary conditions are set to the standard velocity inlet and pressure outlet, while all domain walls are set to the free-slip condition. No-slip boundary conditions are imposed on the hull of the model. The shear stress transport version of the k-ω turbulence model was used to close the RANS equations. The standard volume of fluid (VOF) approach, coupled with a high-resolution interface capturing scheme, was used to capture the free-surface. All degrees of freedom of the the model were constrained to simplify computations. A second-order upwind scheme was used to discretize the convective term and it was integrated in time using a second-order backward differentiating scheme. The *SIMPLE* scheme is used to solve the resulting system of coupled algebraic equations. A time step (Δt) of 0.05 second was chosen based on the *CFL* condition, with 10 inner-iterations. The resulting sway force and yaw moment were obtained by averaging the instantaneous values over a period of 10 seconds once the L_2 norm in the pressure change on the hull reached 10^{-4}. Typical simulations required around 80 seconds of physical time to reach the desired level of convergence.

On top of the previous cases, additional investigations were performed at a $Fr = 0.142$ and a drift angle $\beta = 8°$ to determine the temporal and spatial discretization errors, following the Verification & Validation procedure proposed by Stern et al. (2001). The spatial uncertainties were determined using

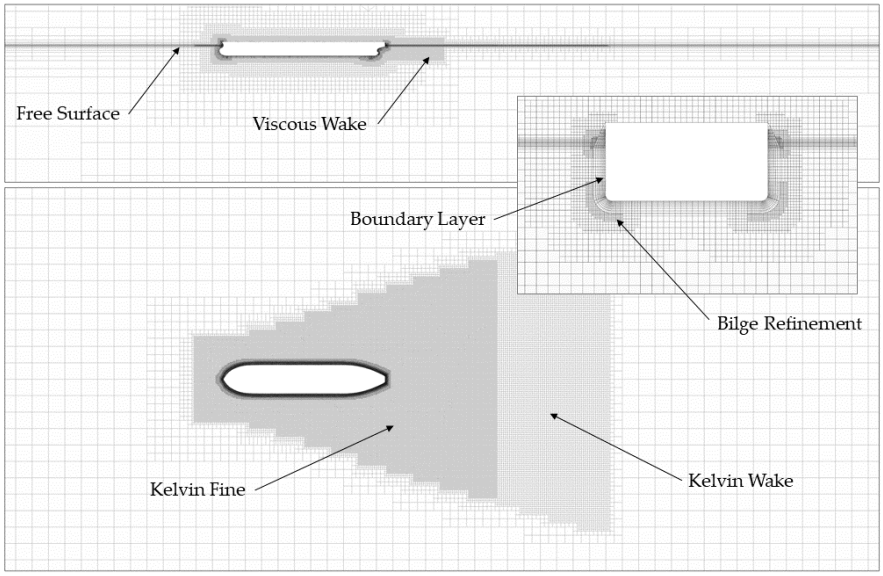

Fig. 1: Standard mesh used for the static drift simulation ($\beta = 0$, $Fr = 0.142$) together with details of the refinements around the model.

Richardson extrapolation (Celik et al. (2008)). The L_2 norm defined earlier was used to quantify the iterative uncertainty, following Eça and Hoekstra (2016). In this regard, a coarser and finer mesh with 2M and 6.3M cells were used. The temporal discretization was not altered for the spatial discretization study. The temporal discretization study was carried out by varying the time-step between 0.025 and 0.1 second, with the number of inner-iterations adjusted to achieve a global iteration count identical between the three cases. To conclude the static drift case, two turbulence models, the Realizable k-ϵ and the Spalart-Allmaras, as well as the double-body approach (no free-surface) were compared. Those simulations used the standard mesh described above, with the exception of the double-body approach that used a different mesh and numerical algorithm (steady simulation).

Planar motion mechanism (PMM) simulations were performed following a similar approach. The motion was achieved using an overset mesh with a total of 6.5M cells. Similar mesh topology to the static drift case was used, with the addition of the overset domain. The coupling between the overset and the background mesh was obtained using linear interpolation. No source or flux correction terms were applied. Both PMM in pure sway and yaw were simulated for oscillatory periods of 6 and 12 seconds. A time-step of 0.005 second was chosen based on the *CFL* condition and motion requirements. This results in a total of 2400 iterations per oscillatory period. Twenty inner-iterations were used within each time-step. Motion for the pure yaw case was imposed so that the centreline of the model was kept tangent to its path at all time. The yaw angle varies as

$$\psi(t) \approx \tan^{-1}\left(\frac{-y_0\omega}{U}\right)\cos(\omega t) = \psi_0\cos(\omega t), \tag{1}$$

where U is the forward speed of the model, y_0 is the sway amplitude and ω is the motion frequency. Simulations are initialized with a straight tow (no motion), until the solution has settled, before imposing the motion. This prevents generating non-physical free-surface oscillations that otherwise travel in the domain and pollute the solution. The manoeuvring coefficients were obtained by an RMS minimization of the error between the measured force/moment and its corresponding Taylor series expansion obtained from the equations of motion, see Oldfield et al. (2016). The same procedure as in the static case was followed for the spatial discretization errors, however, here the manoeuvring coefficients and not the force measured were compared. Turbulence sensitivity was investigated with the Realizable k-ϵ turbulence model. A PMM test in pure sway with an oscillatory period of 12 seconds was chosen for those investigations. The double-body approach was not investigated.

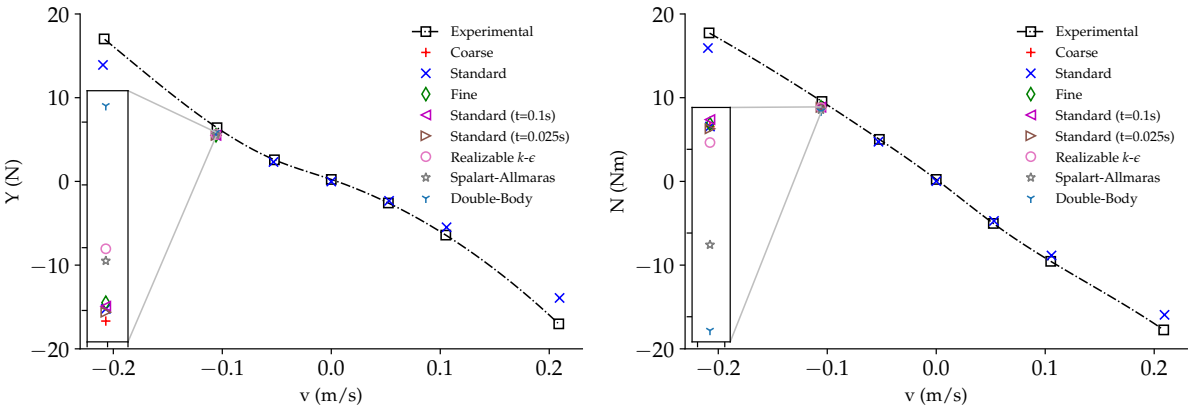

(a) Detail magnification: 75×

(b) Detail magnification: 50×

Fig. 2: Sway force (a) and yaw moment (b) from the static drift simulations against experimental data.

3 Results

The sway force as a function of the drift velocity ($v \equiv -U\sin(\beta)$), is presented on figure 2a. The results for the different spatial and temporal discretizations as well as the different modelling strategies for the chosen test case are also presented. The investigations on the different turbulence models used the same temporal and spatial discretization as the standard case, which was first validated using the procedure described previously. For small drift angles, the agreement with the experimental data is good. For larger drift angles, it can be observed that the agreement deteriorates. The different discretizations, both temporal and spatial, result in very similar values of the sway force. Despite having different formulations, the two additional turbulence models are in good agreement. The largest differences are obtained when the free-surface is omitted. Figure 2b shows the yaw moment as a function of the sway velocity. The yaw moment prediction follows a similar trend as the sway force but under-predicting for the double-body case instead of over-predicting it as in the sway force.

Monotonic convergence is found for the two variables measured (Y, N), with discretization uncertainties of the order of one percent for the standard mesh. Iteration uncertainties were typically lower than the discretization uncertainties by an order of magnitude of two, which allowed to safely neglect them. This results in validation uncertainties of $2.75\%D$ and $0.56\%D$ for the sway force and yaw moment, respectively. The corresponding errors are $14.19\%D$ and $7.25\%D$, so that the results are not validated for the configuration considered ($Fr = 0.142, \beta = 8°$). Comparison on local flow quantities (viscous wake and wave profile) with experimental data show excellent agreement, see figure 3. In the viscous wake, the numerical simulations are able to capture the typical hook-shaped flow structure, and an excellent agreement is obtained in terms of the wave profile along the hull (see figure 3b). It should be noted that despite showing good agreement with the sway force and yaw moment predicted using other models, the Spalart-Allmaras model largely under-predicted the shear stresses on the fore part of the model.

The manoeuvring coefficients are obtained by measuring the slope of the curve shown in figure 2 at the origin. Results are presented in table 1 together with three different sets of experimental data. The first set was obtained from the experimental data presented on figure 2. The yaw moment shows a better agreement with all of the experimental data compared to the sway force.

The results from the PMM simulations are presented in table 2. Coefficients with a subscript v or $\dot{v}$ were obtained from PMM in pure sway whereas the ones with r or $\dot{r}$ were obtained from PMM in pure yaw. In pure sway, the agreement with both sets of experimental results is acceptable. The captured differences are of the same order as the static drift simulation ones. Better agreement is obtained for the larger motion period. Velocity dependent coefficients are shown to agree better with the experimental data, this being more pronounced for the smallest motion period. An acceptable agreement is also noted with the MOERI experimental data, despite being at a different motion period and model scale.

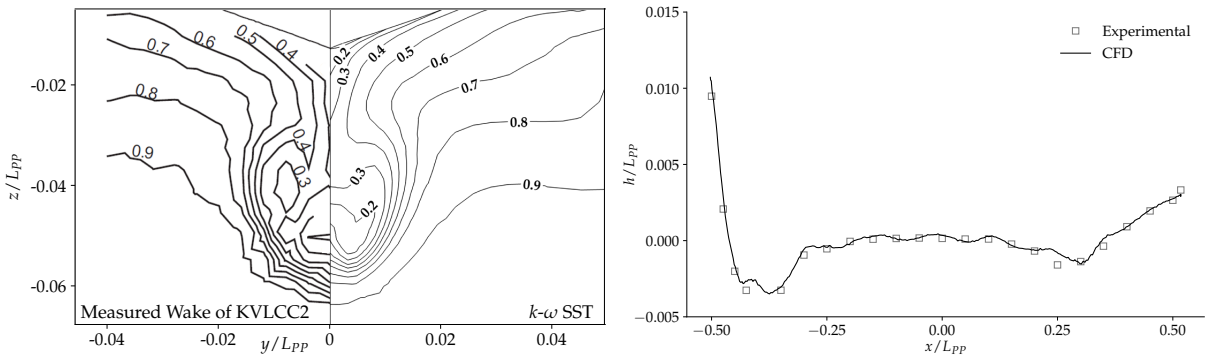

(a) (b)

Fig. 3: Nominal wake (a) and wave profile along model (b) from numerical simulation and experimental measurements (Kume et al. (2006), Kim et al. (2001)).

The different mesh sizes and the turbulence model considered showed an excellent agreement with the baseline simulations (not shown here), with differences in the order of one percent. Iterative uncertainties is found to reach 10^{-3} at the end of each inner-iteration loop, this allows to safely neglect them. Oscillatory convergence is found for all coefficients but $\tilde{N}'_{\dot{v}}$. As a result, Richardson extrapolation cannot be used to estimate the discretization error. This oscillatory behaviour could be due to the limitation of the method used, and not represent an actual oscillation in the convergence of the results, as also noted by Carrica et al. (2016). Despite not being able to rigorously validate the results, we can consider the agreement with experimental data as acceptable for the pure sway case.

The pure yaw motion case has proven to be more challenging to simulate than the pure sway case. This is because of the highly non-linear behaviour of pure yaw compared to pure sway, as documented in Kim et al. (2015). Such different behaviours are also reflected by the poor agreement with the experimental data obtained. Again, angular velocity dependent coefficients are in much better agreement than angular acceleration dependent coefficients. Issues with the post-processing of the experimental data for the pure yaw case at a period of 6 seconds did not allow oscillatory coefficients to be extracted.

4 Concluding Remarks

To conclude this investigation, the following recommendations can be drawn; static drift simulations have shown to yield good results for small drift angles, with the different methods used all being very close, for larger drift angles the agreement deteriorates. This is probably due to the unsteadiness of the flow becoming important and the RANS strategy not being able to capture all the details of the flow. Temporal discretization errors were found to be small, the only noticeable difference in the three time-step was how well the free-surface was captured (not presented here). It can thus be noted that for static drift simulations, at small drift angles, the choice of numerical method does not play a key role in the computation of the coefficients, and all the focus should be on the quality of the mesh to capture all the relevant flow structures. If computational power is an issue, the double-body approach can be considered without too much loss of accuracy, and with a reduction in computation time by a factor of 100.

For planar motion mechanism simulations, similar recommendations can be made for the pure sway

Table 1: Manoeuvring coefficients from static drift simulations against experimental data.

Coefficient	Present (CFD)	NMRI (EFD) (SIMMAN (2014))	MOERI (EFD) (He et al. (2016))	Kume et al. (2006) (EFD)
Y'_v (ϵ %D)[a]	-0.01362	-0.01535 (-11.27)	-0.01619 ((-15.87)	-0.01838 (-25.89)
N'_v (ϵ %D)	-0.00954	-0.01027 (-7.11)	-0.00875 (9.03)	-0.01064 (-10.34)

[a] ϵ defined as the relative error between numerical simulations and experimental results.

Table 2: Manoeuvring coefficients from PMM simulations against experimental data. The tilde above each coefficient emphasises their frequency-dependence.

Coefficient	Present (CFD)		NMRI (EFD)		MOERI (EFD)
	Period: 12 s	6 s	12 s	6 s	10 s
$\tilde{Y}'_v$ (ϵ %D)[a]	-0.01367	-0.01438	-0.01519 (-10.00)	-0.01638 (-12.21)	-0.01619 (-15.56)
$\tilde{Y}'_{\dot{v}}$ (ϵ %D)	-0.01419	-0.01470	-0.01439 (-1.39)	-0.01868 (-21.31)	-0.015104 (-6.05)
$\tilde{N}'_v$ (ϵ %D)	-0.00998	-0.01076	-0.01070 (-6.72)	-0.01318 (-18.36)	-0.00875 (14.05)
$\tilde{N}'_{\dot{v}}$ (ϵ %D)	-0.00046	-0.00042	-0.00051 (-9.80)	-0.00076 (-44.76)	-0.00078 (-41.02)
$\tilde{Y}'_r$ (ϵ %D)	0.00286	0.00269	0.00430 (-33.48)	[b]	0.00472 (-39.41)
$\tilde{Y}'_{\dot{r}}$ (ϵ %D)	-0.00056	-0.00051	-0.00312 (-82.05)	[b]	-0.00142 (-60.56)
$\tilde{N}'_r$ (ϵ %D)	-0.00213	-0.00246	-0.00252 (-15.47)	[b]	-0.00311 (-31.51)
$\tilde{N}'_{\dot{r}}$ (ϵ %D)	-0.00067	-0.00101	-0.00113 (-40.70)	[b]	-0.00080 (-16.25)

[a] ϵ defined as the relative error between numerical simulations and experimental results.
[b] Raw experimental data is problematic.

case, however, this time proper initialisation of the solution is necessary. This only needs to be done once, and the resulting initialised field can be used to start all required cases. In the pure yaw case, more investigations are required, the coefficients obtained do not agree well with experimental data. This arise from much more non-linearities and unsteadiness in the flow generated by this motion. This seems to be a general issue in manoeuvring simulations (Kim et al. (2015)). The method used to derive the oscillatory coefficients is believed to be a better representation than computing the coefficients at a single point.

5 Acknowledgements

The author would like to thanks Prof. Pandeli Temarel for his help during the conduction of this master project as well as Mr. Bernat Font Garcia and Dr. Gabriel Weymouth for their useful comments on an early version of this extended abstract.

References

C. Oldfield, M.M. Larmaei, A. Kendrick, K. McTaggart (2015). Prediction of Warship Manoeuvring Coefficients using CFD. *World Maritime Technology Conference*.

F. Stern, R.V. Wilson, H.W. Coleman, E.G. Paterson (2001). Comprehensive approach to verification and validation of CFD simulations-part 1: methodology and procedures. *Journal of Fluid Engineering*, **123**(4), 793–802.

H. Kim, H. Akimoto, H. Islam (2015). Estimation of the hydrodynamic derivatives by RANS simulation of planar motion mechanism test. *Journal of Ocean Engineering*, **108**, 129–139.

I.B. Celik, U. Ghia, P.J. Roache, C.J. Freitas, H. Coleman, P.E. Raad (2008). Procedure for estimation and reporting of uncertainty due to discretization in CFD applications. *Journal of Fluids Engineering*, **130**(7).

K. Kume, J. Hasegawa, Y. Tsukada, J. Fujisawa, R. Fukasawa, M. Hinatsu (2006). Measurements of hydrodynamic forces, surface pressure, and wake for obliquely towed tanker model and uncertainty analysis for CFD validation. *Journal of Marine Science and Technology*, **12**(2), 65–75.

L. Eça, M. Hoekstra. (2006). On the influence of the iterative error in the numerical uncertainty of ship viscous flow calculations. *26th Symposium on Naval Hydrodynamics*, 17–22

L. Zou, L. Larsson, M. Orych (2010). Verification and validation of CFD predictions for a manoeuvring tanker. *Journal of Hydrodynamics, Ser. B*, **22**(5), 438–445.

P.M. Carrica,A. Mofidi, K. Eloot, G. Delefortrie (2016). Direct simulation and experimental study of zigzag maneuver of KCS in shallow water. *Ocean Engineering*, **112**, 117–133.

S. He, P. Kellett, and Z. Yuan, A. Incecik, O. Turan, E. Boulougouris (2016). Manoeuvring prediction based on CFD generated derivatives. *Journal of Hydrodynamics, Ser. B*, **28**(2), 284–292.

SIMMAN (2014). Workshop on Verification and Validation of Ship Manoeuvring Simulation Methods.

W.J. Kim, S.H. Van, D.H. Kim, D (2001). Measurement of flows around modern commercial ship models. *Experiments in fluids*, **31**(5), 567–578